Immunology Letters 206 (2019) 1–10

Contents lists available at ScienceDirect

Immunology Letters

journal homepage: www.elsevier.com/locate/immlet

miR-181b regulates ER stress induced neuron death through targeting Heat Shock Protein A5 following intracerebral haemorrhage

Zhenyu Wang[a], Liang Fang[b], Hui Shi[b], Zhao Yang[b,*]

[a] Department of Rehabilitation Medicine, Yongchuan Hospital, Chongqing Medical University, Chongqing, 402160, China
[b] Department of Neurology, Yongchuan Hospital, Chongqing Medical University, Chongqing, 402160, China

ARTICLE INFO

Keywords:
miR-181b
ER stress
Neuron death
Heat Shock Protein A5
ICH

ABSTRACT

Endoplasmic reticulum (ER) stress acts as a protein folding and contributes to neuronal damage and neurological deterioration following intracerebral hemorrhage (ICH). Heat Shock Protein A5 (HSPA5) serves as an essential regulator of the endoplasmic reticulum (ER) stress response. However, the specific mechanism has not been will identified. Primary cortical neurons from C57BL/6 mice were subjected to erythrocyte lysates. Cell viability, microRNA and HSPA5 levels, and ER stress was detected. The interaction between microRNA and the target HSPA5 was identified by dual luciferase reporter gene assay. In addition, inflammatory cytokines, brain edema, and neurological functions in ICH mice were also assessed. Erythrocyte lysates induced ER stress and neuron damage, downregulated miR-181b and upregulated HSPA5 levels. MiR-181b suppressed HSPA5 expression by directly binding its 3′-untranslated region. Correspondingly, our data demonstrated that overexpression of miR-181b attenuated erythrocyte lysates induced neuronal necrosis and apoptosis. In vivo, downregulated miR-181b increased the HSPA5 level, along with significant elevations of pro-inflammatory cytokines, brain edema, and neurological injury following ICH. HSPA5 pathway plays an important role in ER stress induced brain damage following ICH. In addition, miR-181b has neuroprotective effects that alleviates neurological injury and represents a promising therapeutic strategy in ICH.

1. Introduction

Intracerebral hemorrhage (ICH) is the common subtype of stroke and represents approximately 10% to 20% of all strokes [1–3]. ICH is characterized by high rates of mortality and disability, and little effective therapeutic strategies are available currently [4–6]. Apart from the nature of the hematoma, like volume and position, some other factors have been identified to be associated with the prognosis of ICH [7]. Nemours evidence supports that inflammatory response plays a key role in ICH [8,9].

The endoplasmic reticulum (ER) is an organelle wherein proteins are constructed and produced [10]. The accumulation of misfolded/unfolded proteins induce ER dysfunction is characterized as ER stress [11–13]. ER stress is one of the factors that lead to cell apoptosis [14–16]. Several studies demonstrate that ER stress contributes to ICH [17–19].

Micro-RNAs (miRNAs) are small, noncoding endogenous RNA molecules conserved through the biology evolution [20–22]. They inhibit the target mRNA by binding to the complementary sequences in the 3'-UTRs of mRNAs, result in translational inhibition or mRNA degradation [23–25]. miRNAs play vital roles in physiology and pathology of ICH [26,27]. Several studies suggest that miRNAs have acted as key factors to regulate neuroprotection or neuronal damage in ICH [28,29].

By using miRNA microarrays, we have identified miR-181b was downregulated in erythrocyte lysates treated neurons, and predicted miR-181b targeting HSPA5 by bioinformatics analysis. This experiment further examines the role of miR-181b in erythrocyte lysates-treated primary cortical neurons in vitro and in ICH mice in vivo.

2. Materials and methods

2.1. Animals

8 week-old male specific pathogen-free (SPF) C57BL/6 mice were purchased from Chongqing Medical University and were housed in standard polypropylene cages at the animal facility until the day of the experiment. All procedures were performed in accordance with guidelines established by the Animal Care and Use Committee of Chongqing Medical University.

* Corresponding author.
E-mail address: yangzhao5140@sohu.com (Z. Yang).

https://doi.org/10.1016/j.imlet.2018.11.014
Received 29 September 2018; Received in revised form 1 November 2018; Accepted 28 November 2018
Available online 29 November 2018

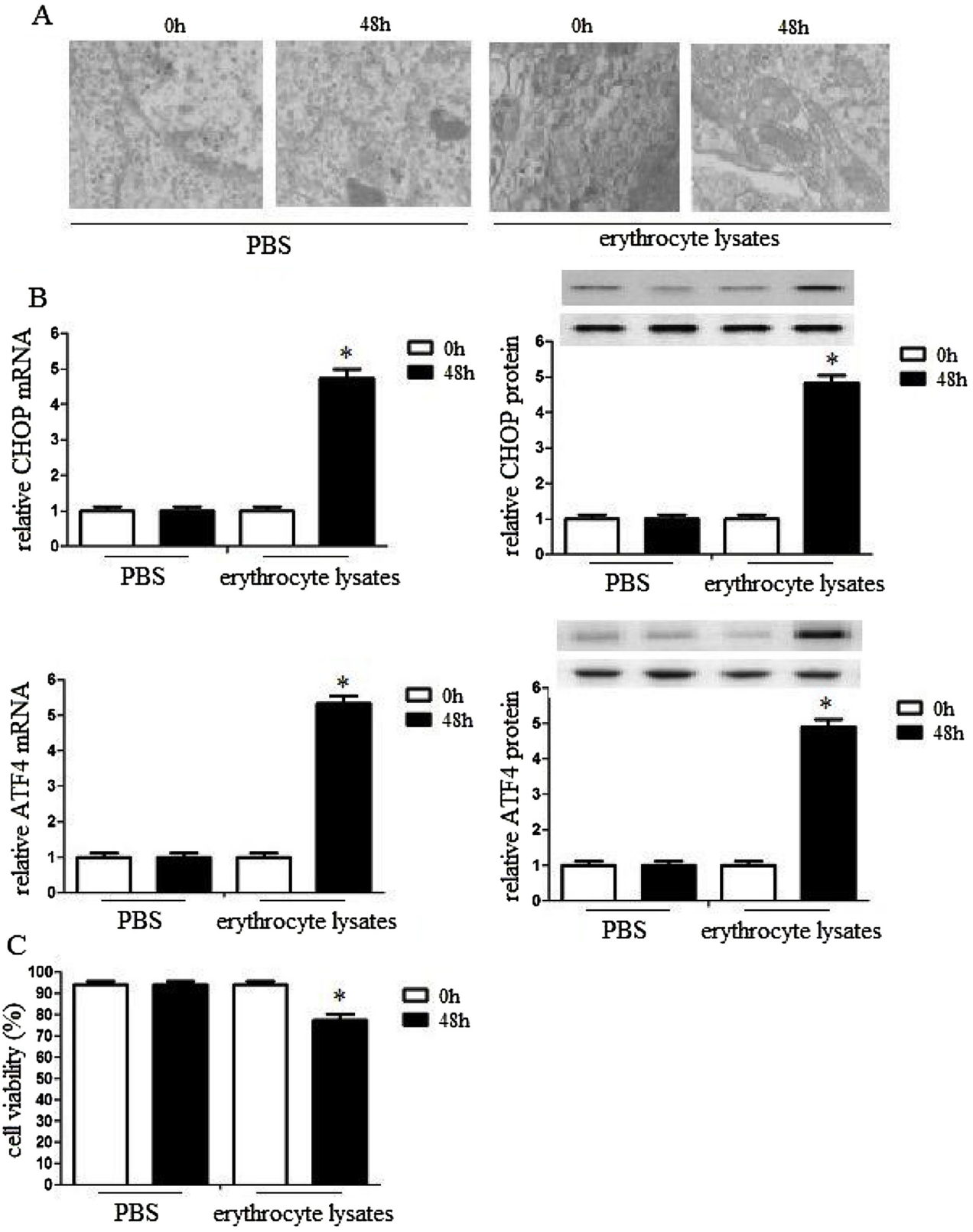

Fig. 1. Erythrocyte lysates induced ER stress and damage of neurons in vitro.
Neurons (1×10^5) were stimulated with 10 µl PBS or erythrocyte lysates for 48 h. (A) Neurons were directly fixed with 1% glutaraldehyde and postfixed with 2% osmium tetraoxide. Lipid droplet formation was observed. (B) ER stress related protein CHOP and ATF4 levels were determined by qRT-PCR and western blot. (C) MTT reagent was added and the cell viability was assessed. Experiments performed in triplicate showed consistent results. Data are presented as the mean ± SD of three independent experiments. *$P < 0.05$.

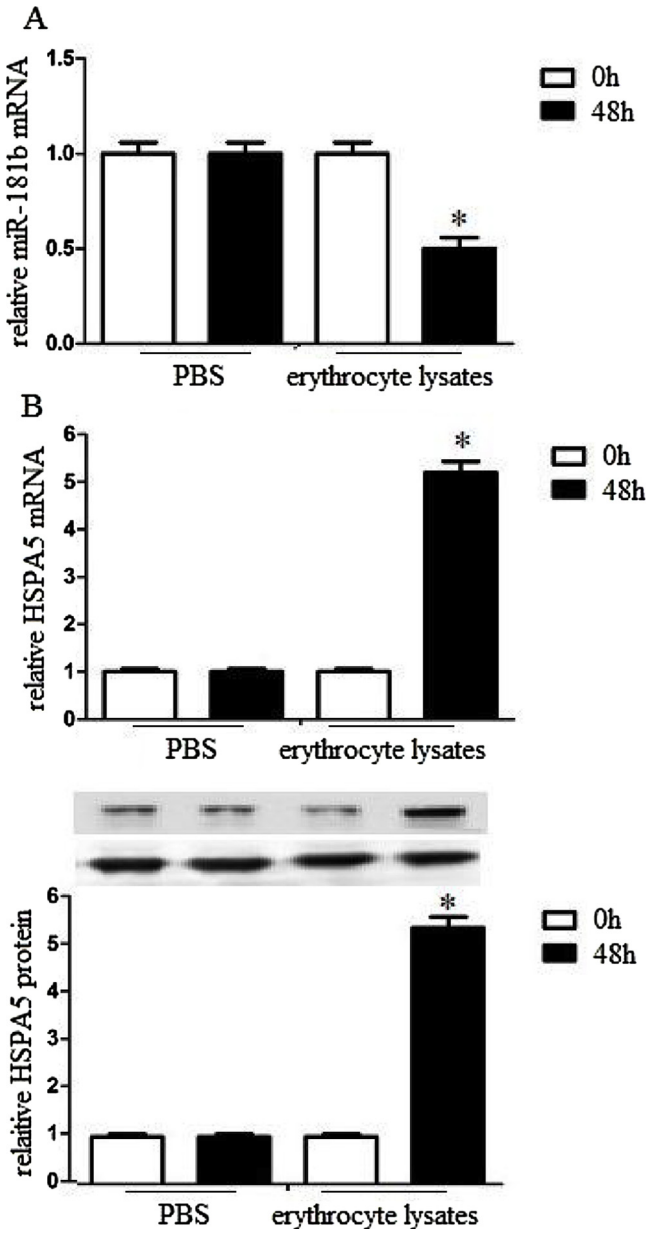

Fig. 2. Erythrocyte lysates downregulated miR-181b and upregulated HSPA5 levels of neurons.
Neurons (1×10^5) were stimulated with 10 μl PBS or erythrocyte lysates for 48 h. (A) miR-181b mRNA levels were evaluated by quantitative RT-PCR. (B) HSPA5 mRNA and protein levels were evaluated by quantitative RT-PCR and western blots. Experiments performed in triplicate showed consistent results. Data are presented as the mean ± SD of three independent experiments. *$P < 0.05$.

2.2. Primary neuronal cell culture

Primary cortical neurons were prepared from whole cerebral cortices of C57BL/6 mouse embryos (E16). After removal of the meninges, tissue was digested by 0.005% trypsin/0.002% EDTA (10 min, 37 °C), mechanically dissociated, and centrifuged at 1000 *g* for 5 min. The cell pellet was resuspended in neurobasal medium (Gibco, Oakland, CA, USA) containing B27 serum free supplement (Gibco) and 500 nM L-glutamine. A total of 2×10^5 cells per well were seeded on sterile poly-L-lysine (Sigma-Aldrich, Saint Louis, MO, USA) coated glass coverslips in a 24-well plate and incubated at 37 °C and 5% CO_2. After 1 h, culture medium was changed completely. Purity of neuronal cultures was > 95% as confirmed by random staining with neuronal and glia markers. Five days after plating, neurones had developed a dense network of extensions.

2.3. Preparation of erythrocyte lysates

Mice were anesthetized at 3 days after ICH. Mice were directly decapitated, and the spleen was removed from C57BL/6 mice. Single-cell suspensions of splenocytes were prepared using stainless steel mesh screens. And then, 1×10^5 splenocytes were incubated with 1 ml red blood cell lysing solution for 20 min, and centrifuged at 2000 rpm for 10 min. The supernatants were utilized as erythrocyte lysates.

2.4. Cell treatment

Neurons (1×10^5) were stimulated with 10 μl PBS or erythrocyte lysates for 48 h. After then, the supernatants were removed and further analyzed for cytokine production with ELISA.

2.5. Intracerebral hemorrhage model

Briefly, mice were anesthetized with an intraperitoneal injection of 400 mg/kg chloral hydrate and fixed on a mouse stereotaxic frame (Stoelting). A 20-μl volume of autologous non-anti-coagulated blood was collected from the tail vein of the mouse and then injected into the caudate nucleus at 2 μl/min under stereotactic guidance at the following coordinates relative to bregma: 0.8 mm anterior, 2 mm left lateral, and 3.5 mm deep during a period of 10 min. The needle was held in place for 10 min after injection, and the microsyringe was pulled out after the blood had coagulated. The craniotomy was then sealed with bone wax, and the scalp was closed with sutures. Body temperature was maintained at 37 °C throughout the procedure, and the mice were given free access to food and water after they woke up. The mice that died because of anesthesia were excluded.

2.6. Immunochemistry staining

Mice were anesthetized at 3 days after ICH. Mice were directly decapitated, and their brains were obtained to store at −80 °C for use for further analysis. These mice underwent transcardial perfusion with 200 ml of phosphate-buffered saline (PBS), followed by 100 ml of 4% paraformaldehyde (PFA) in 0.1 M PBS. The brains were removed and postfixed for 24 h in 4% PFA and then were placed in 30% sucrose until sinking. Coronal brain sections of 10 μm thickness were obtained with a freezing microtome (Leica, Nussloch, Germany) and were kept at −20 °C for immunofluorescence. After being washed in PBS for 10 min, the sections were incubated with 5% bovine serum albumin for 60 min in order to block the nonspecific binding and then were incubated with goat anti-mouse ionized calcium-binding adapter molecule 1 (Iba-1) primary antibody (1:100; R&D Systems, Minneapolis, MN, USA)at 4 °C all the night. After being washed three times with PBS, the sections were incubated with secondary antibody IgG (1:100; KPL, MD, USA) for 60 min at the room temperature. The sections were rinsed three times for 5 min and were cover slipped with a ProLong antifade medium (Molecular Probes, Eugene, OR, USA). The Iba-1-positive cells were visualized using a microscope (OlympusBX51, Japan). Foreachanimal, six representative sections of each brain were selected. IPP6.0 image processing software (Media Cybernetics, MD, USA) was utilized to count the number of positive cells.

2.7. Tissue preparation

Mice were anesthetized at 3 days after ICH. Mice were directly decapitated, and their brains were obtained to store at −80 °C for use for further analysis. The brain was extracted and placed on ice. Using the needle track as the center, to prepare a coronal section and a sagittal

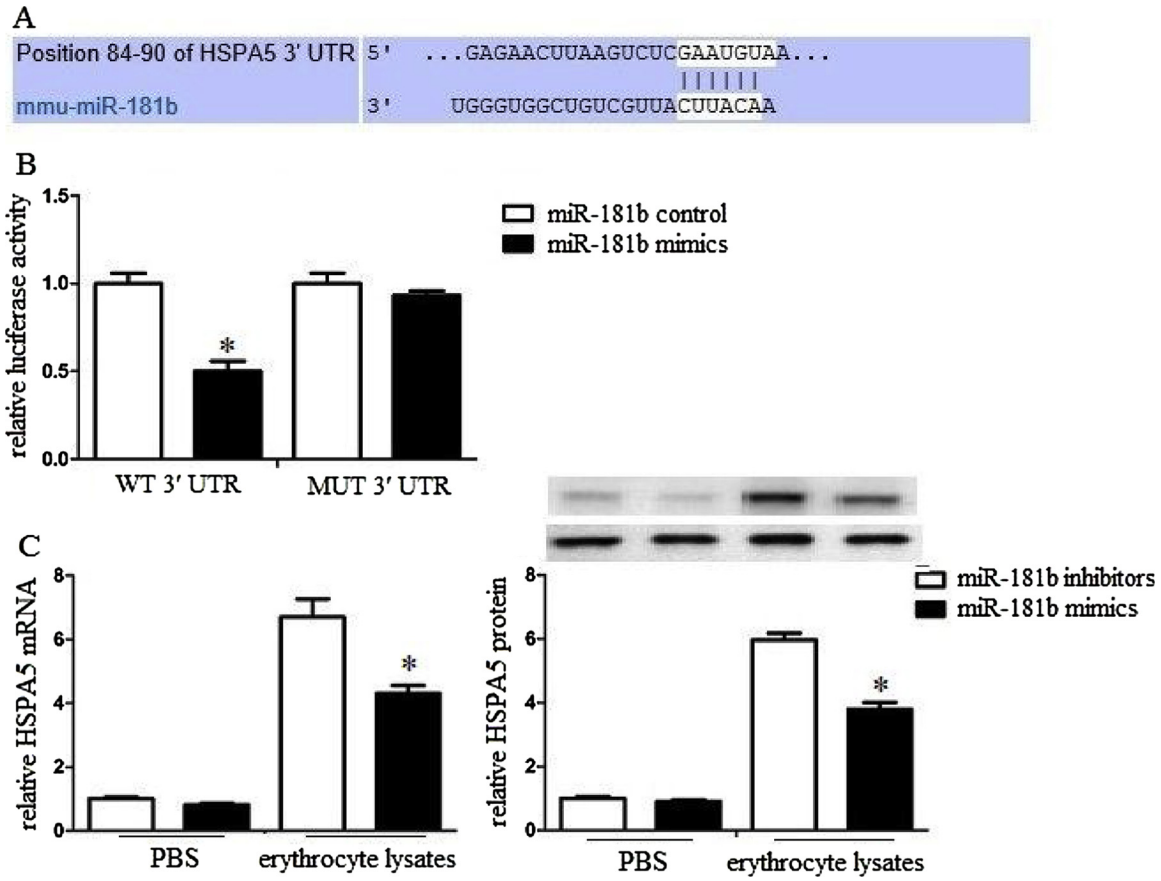

Fig. 3. HSPA5 was a direct target of miR-181b of neurons.
(A) A HSPA5 3′ UTR fragment containing wild-type or mutant miR-181b binding sites was cloned downstream of the luciferase reporter gene. The region of the HSPA5 mRNA 3′ UTR predicted to be targeted by miR-181b as indicated. (B) Luciferase activity assays using reporters with wild-type or mutant HSPA5 3′ UTRs were performed after cotransfection with miR-181b mimics or control in neurons. The luciferase activity of the control transfection in each experiment was used to normalize the data, and the luciferase activity of the control transfection was set equal to 1. (C) Neurons (1×10^5) were transduced with miR-181b mimics or inhibitors, and then cells were treated with PBS or erythrocyte lysates. After 48 h, cells were harvested, and HSPA5 levels were analyzed with qRT-PCR and western blot assays. Experiments performed in triplicate showed consistent results. Data are presented as the mean ± SD of three independent experiments. *P < 0.05.

section, the brain was cut and divided into four parts on the hematoma side: anterior-inner, anterior-outside, posterior-inner, and posterior-outside. From each of these quadrants, a total of 5 mm of brain tissue surrounding the hematoma was collected to further analysis.

2.8. qRT-PCR

Mice were anesthetized at 3 days after ICH. Mice were directly decapitated, and their brains were obtained to store at −80 °C for use for further analysis. Brain tissues were dissolved in TRIzol reagent (Invitrogen, Carlsbad, CA, USA) and total RNA was extracted and subjected to RT-PCR using the PrimeScript RT reagents kit (TaKaRa, Shiga, Japan) according to the manufacturer's directions. qPCR was performed using the SYBR Premix Ex Taq polymerase (TaKaRa). Fluorescence signals were measured after 40 PCR cycles, and all samples were normalized to β-actin RNA content. The mouse specific primers are as follows: HSPA5, 5′-CCGC TCGAGGTGCACTGATCTGCTAG AGCTGTA -3′(forward), 5′-GAATGCGGCCGCCAGTCTTAAATTTTAGTT ATCTAAAATAAAAGATGG-3′ (reverse); ATF4, 5′- CCCCTTCACCTTCT TACAACC -3′(forward), 5′-GGG C TCATACAGATGCCACTA -3′ (reverse); CHOP, 5′- AATCAG AG CT GGAACCTGAGGA -3′ (forward), 5′-TGCT TT CA GG TGT GGT GATGTATG -3′ (reverse); β-actin, 5′- CTA CAAT GAGC TGCGTGTGG -3′ (forward); 5′- AAGGAAGGCTGGAAGAG TGC-3′ (reverse); Experiments were carried out in triplicate for each data point. A threshold cycle value (CT) was calculated by the $^{\Delta\Delta}$CT method. The data were analyzed by using Light Cycler Software 4.0 (Roche Diagnostics). All samples were run in duplicate.

2.9. Enzyme-linked immunosorbent assay

The perihematomal region of each ipsilateral hemisphere used for cytokine/chemokine quantification was homogenized and sonicated in RIPA buffer (Cell Signaling) with protease inhibitors, then centrifuged at 14,000 × *g*. The protein concentration of the supernatant was determined using the BCA Protein Assay Kit (Thermo Fisher Scientific Inc.). 100 μg total protein was used for cytokine/chemokine quantification by multiplex ELISA (mouse inflammation panel I, Millipore) according to manufacturer's instructions.

2.10. Western blot

Mice were anesthetized at 3 days after ICH. Mice were directly decapitated, and their brains were obtained to store at −80 °C for use for further analysis. Total protein was extracted from brain tissue using T-PER Tissue Protein Extraction Reagent (Pierce, Rockford, IL, USA) and quantified with BCA Protein Assay (Pierce). The proteins were separated by 16% sodium dodecyl sulfate-polyacrylamide gel electrophoresis. Proteins were transferred onto polyvinylidene difluoride filters (PVDF) membranes, followed by blocking with 5% milk for 1 h at room temperature. Then, specific primary antibodies were incubated overnight at 4 °C. After the incubation with secondary antibodies for 1 h, we used ECL (Thermo Scientific; PI32109) to visualize bands,

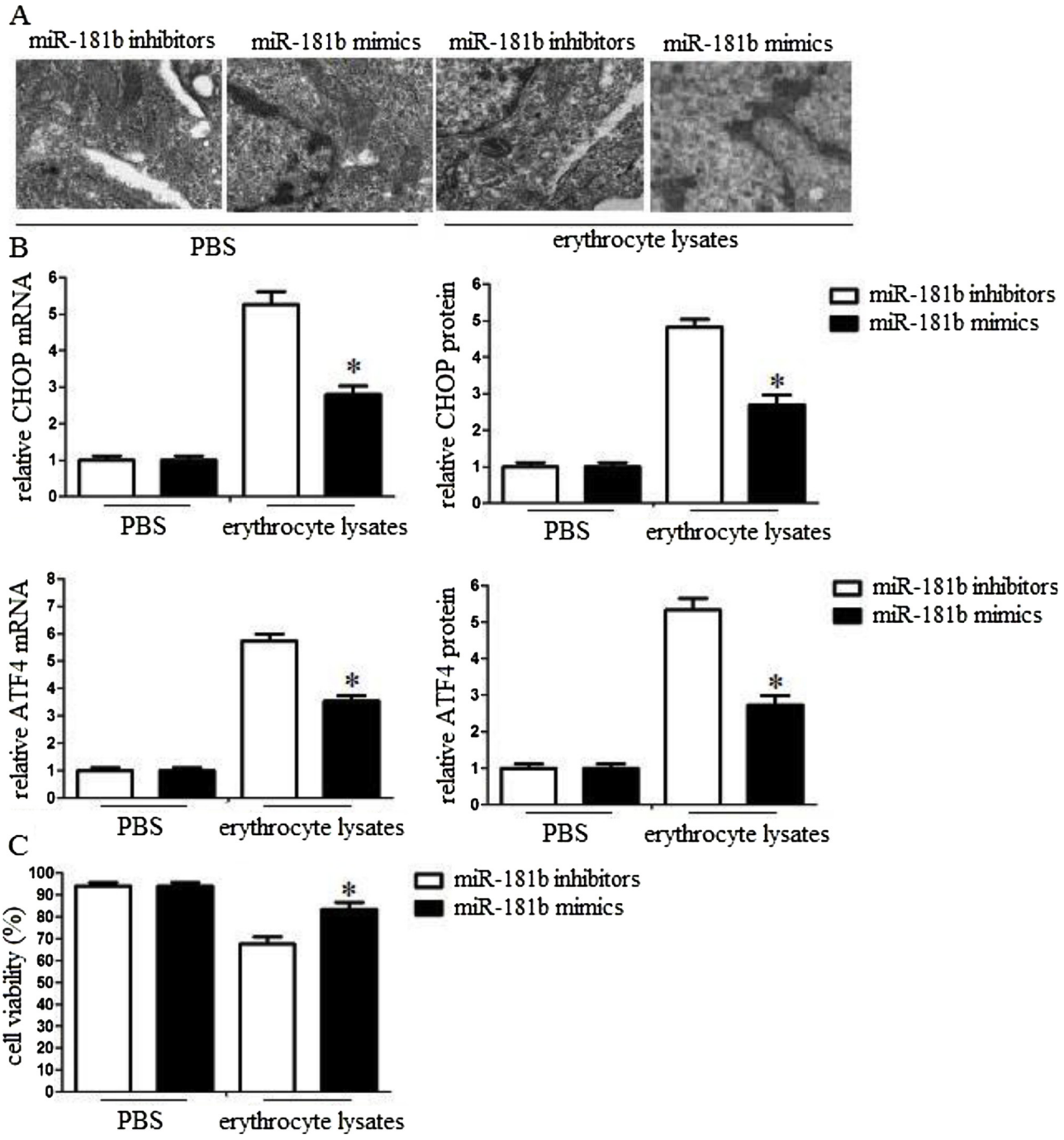

Fig. 4. miR-181b attenuated ER stress and damage of neurons in vitro.
Neurons (1×10^5) were transduced with miR-181b mimics or inhibitors for 48 h, then the cells were stimulated with 10 μl PBS or erythrocyte lysates for 48 h. (A) Neurons were directly fixed with 1% glutaraldehyde and postfixed with 2% osmium tetraoxide. Lipid droplet formation was observed. (B) ER stress related protein CHOP and ATF4 levels were determined by qRT-PCR and western blot. (C) MTT reagent was added and the cell viability was assessed. Experiments performed in triplicate showed consistent results. Data are presented as the mean ± SD of three independent experiments. *$P < 0.05$.

which were then analyzed by the Quantity One (Bio-Rad; Version 4.6.2).

2.11. Cell viability assessment

Cell viability of neuron was assessed using 3-(4,5- dimethyl- 2-thiazolyl) -2,5-diphenyl-2H-tetrazolium bromide (MTT, Sigma-Aldrich) assay. After 48 h, MTT reagent was added to the wells, incubated for 4 h at 37 °C, 5% CO_2. After centrifugation, the supernatant was removed from each well. The coloured formazan crystal produced from MTT was dissolved with 0.15 ml DMSO, thentheopticaldensity(OD) value A490 was measured by the multiscanner autoreader (Dynatech MR 5000; Dynatech Laboratories, Chantilly, VA, USA). The absorbance was measured at 570 nm. The mean of readings of triplicate wells was taken as one value. The OD value for the control cultures was considered as 100% viability and viability in other samples is expressed as a percentage of viability in the control cultures.

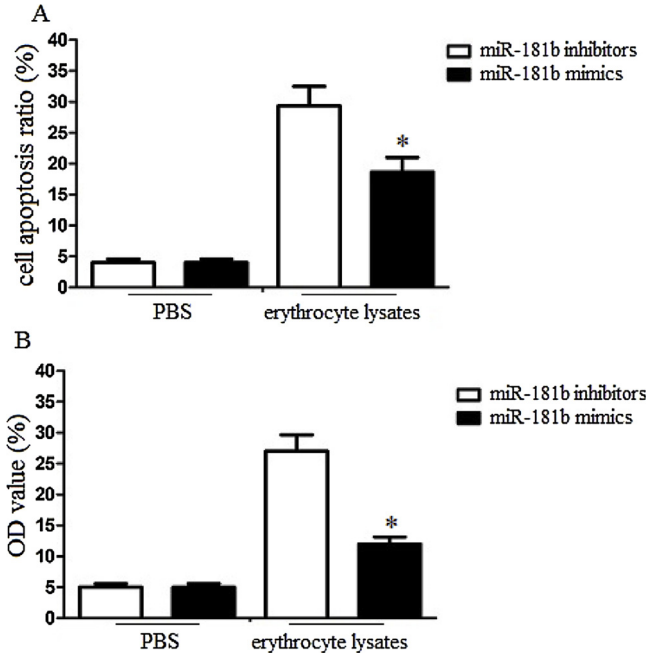

Fig. 5. miR-181b attenuated apoptosis of neurons in vitro.
Neurons (1×10^5) were transduced with miR-181b or inhibitors for 48 h, then the cells were stimulated with 10 μl PBS or erythrocyte lysates for 48 h. (A) Cell apoptosis ratio was detected by flow cytometry. Apoptosis cells were determined by AnnexinV positive and propidium iodide (PI) negative cells. (B) The ApoAlert caspase-3 colorimetric assay kit (Clontech, Palo Alto, USA) was used. Hydrolysed pNA was detected using a Multiscan MS colorimeter (Thermo Labsystems, Vantaa, Finland) at 405 nm. Experiments performed in triplicate showed consistent results. Data are presented as the mean ± SD of three independent experiments. *$P < 0.05$.

2.12. Flow cytometric analysis of apoptosis

An annexin V-fluorescein isothiocyanate (FITC) apoptosis detection kit (Oncogene Research Products, Boston, MA, USA) was used to detect apoptosis. The cells were seeded in 100-ml flasks and incubated until there was about 90% confluence in DMEM supplemented with 10% foetal bovine serum. Then the cells were harvested, washed with ice-cold PBS twice, and resuspended in binding buffer (10 mM of Hepes, pH 7.4, 1.50 mM of NaCL (2.5 Mm of $CaCL_2$, 1 mM of $MgCL_2$, 4% bovine serum albumin. Annexin V-fluorescein isothiocyanate (0.5 mg/ml) and propidium iodide (0.6 mg/ml) were then added to a 250-ml aliquot (1×10^6 cells) of this cell suspension according to the protocol of the manufacturer. After a 15-min incubation in the dark at room temperature, stained cells were immediately analyzed on a flow cytometer (Beck-man Coulter, Fullerton, CA, USA). All of the samples were assayed in triplicate, and the cell apoptosis rate calculated using the following formula: apoptosis rate = (apoptotic cell number/total cell number) × 100%.

2.13. Caspase assay

To analyze caspase-3-like protease activities, the ApoAlert caspase-3 colorimetric assay kit (Clontech, Palo Alto, USA) was utilized. Cytosolic lysates were prepared 48 h following transfec-tion and incubated with 50 mm p-nitroanilide (pNA) conjugated to the caspase cleavage site Asp-Glu-Val-Asp (DEVD) for 1 h at 37 °C. Hydrolyzed pNA was detected using a Multiscan MS colorimeter (Thermo Labsystems, Vantaa, Finland) at 405 nm. For control experiments, the lysates were incubated with 10 mm of the caspase-3 inhibitor DEVD-fmk (Clontech) for 30 min, before addition of the substrate.

2.14. Transmission electron microscopy

Neurons were collected and fixed in a solution containing 2% paraformaldehyde and 0.1% glutaraldehyde in 0.1 M sodium cacodylate for 2 h, postfixed with 1% OsO_4 for 1 h, washed and stained in 3% aqueous uranyl acetate for 1 h. The samples were then washed again, dehydrated with a graded alcohol series, and embedded in Epon-Araldite resin. Ultrathin sections were cut on a Reichert ultramicrotome, counterstained with 0.3% lead citrate and examined on a Philips EM420 electron microscope.

2.15. Plasmid construction and luciferase assays

A fragment from the 3′-UTR of the HSPA5 gene containing miR-181b binding sites was amplified by PCR and then cloned into the pmiR-RB-REPORTTM vector (RiboBio, Guangzhou, China). The following primer sets were used to generate specific fragments: Hspa5 3′-UTR forward, 5′-CCGCTCGAGGTGCACTGATCTGCTAGAGCTGTA-3′; Hspa5 3′ -UTR reverse, 5′-GAATGCGGCCGCCAGTCTTAAATTTTAGTT ATCTAAAATAAAAGATGG-3′. We also generated mutant 3′-UTR of the HSPA5 gene with substitution of 7 bp from the seed region of the predicted miR-181b binding sites. Both segments were confirmed by sequencing.

Mouse cortical neurons were plated at a density of 0.5×10^5 cells per well in 24-well plates 1 day before transfection. Cells were co-transfected with pmiR-RB-REPORT vector, including the 3′-UTR of HSPA5 (with either wild-type or mutant miR-181b binding sites), and pre-miR-181b or negative control plasmid with Lipofectamine 2000 (Invitrogen). Luciferase assays were performed with the dual-luciferase reporter assay system (Promega) 48 h after transfection, according to the manufacturer's protocols.

2.16. Oligonucleotide transfection

Neurons were transduced with 50 nmol/l of miRNA mimics and with 50 nmol/l of RNA duplexes according to the manufacturer's protocol (Applied Biosystems, Carlsbad, CA). After cocluture for 6 h, the fresh medium was added. And then, 24 h after transfection, neurons were collected and utilized for further analysis such as RT-PCR or western blot. Neurons were trypsinized to identify the viability over 90%.

2.17. Intracerebroventricular injection

The in vivo transfection was performed according to the method described as follows: the stereotaxic coordinates were 0.5 mm posterior and 1.0 mm lateral to bregma and 2.5–3.0 mm ventral to the surface of the skull. The miR-181b mimics or miR-367 control (2 μg/2 μl) were added to 1.25 μl of Entranster™ in vivo transfection reagent. The solution was mixed gently, left for 15 min and then injected intracerebroventricularly (i.c.v.) using a micro syringe (Hamilton, NV, USA) under the guidance of the stereotaxic instrument (RWD Life Science).

2.18. Evaluation of neurological scores

The neurological scores were assessed by Neurological Severity Scores, according to the motor, sensory, reflex, and balance tests. Neurological function was assessed on a scale of 1–18; a score of 1 point is regarded as the inability to perform the test or for the lack of a tested reflex. The higher the score, the more severe the injury (normal score: 2–3; maximal deficit score: 18).

2.19. Measurement of brain edema

Brain hemisphere were quickly separated and weighted to assess the

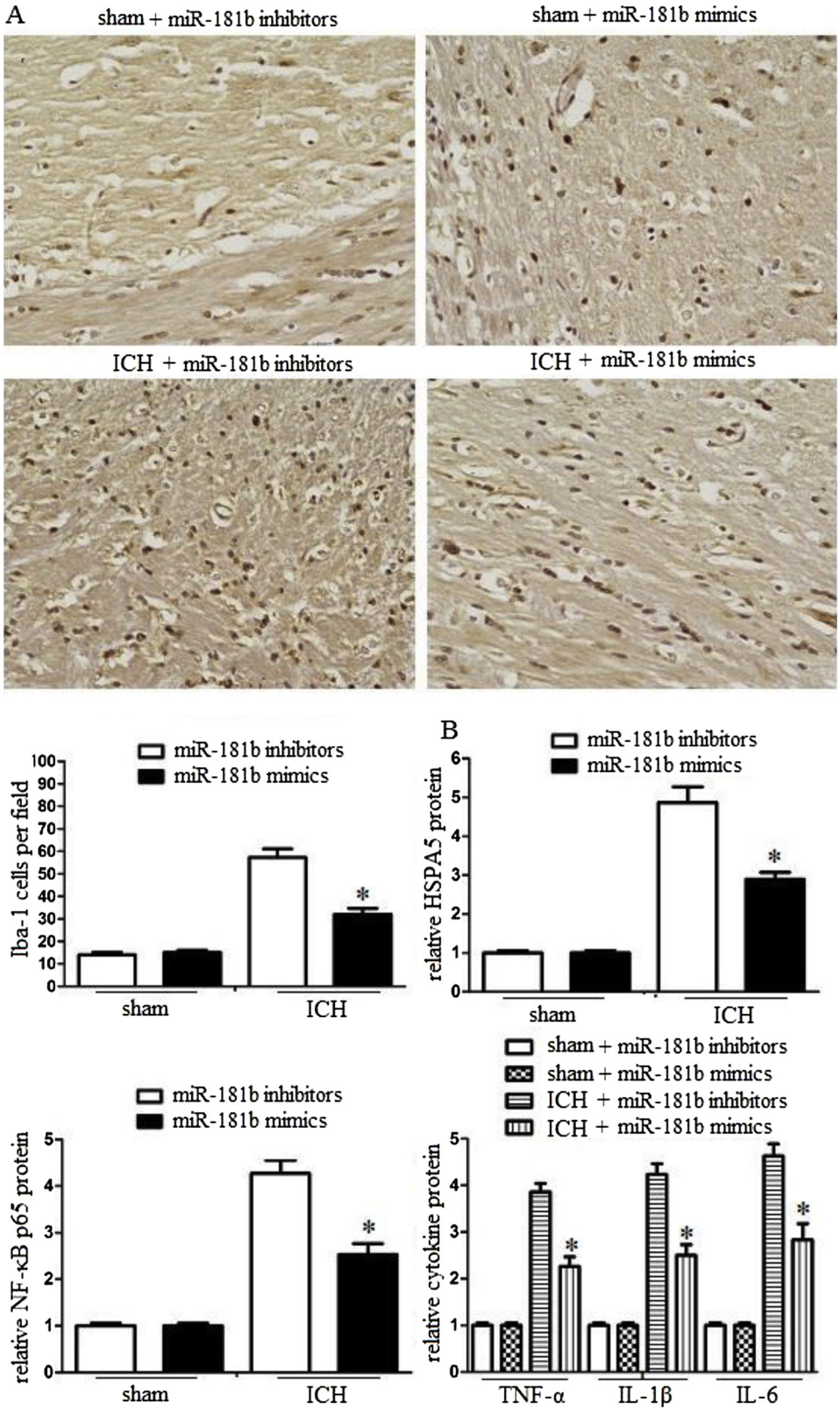

Fig. 6. miR-181b attenuated inflammation in vivo.
Mice were received an intracerebral ventricular injection of miR-181b mimics or inhibitors 10 min after ICH and sacrificed 48 h after ICH. The brains were dissected. (A) The perihematomal region of cerebral tissue was collected, and microglia was analyzed with anti-Iba-1 antibody (× 400 magnification). (B) HSPA5, NF-κB p65, and inflammatory cytokine levels of perihematoma tissue of ICH mice were assayed by western blotting. Experiments performed in triplicate showed consistent results. Data are presented as the mean ± SD of three independent experiments. *P < 0.05.

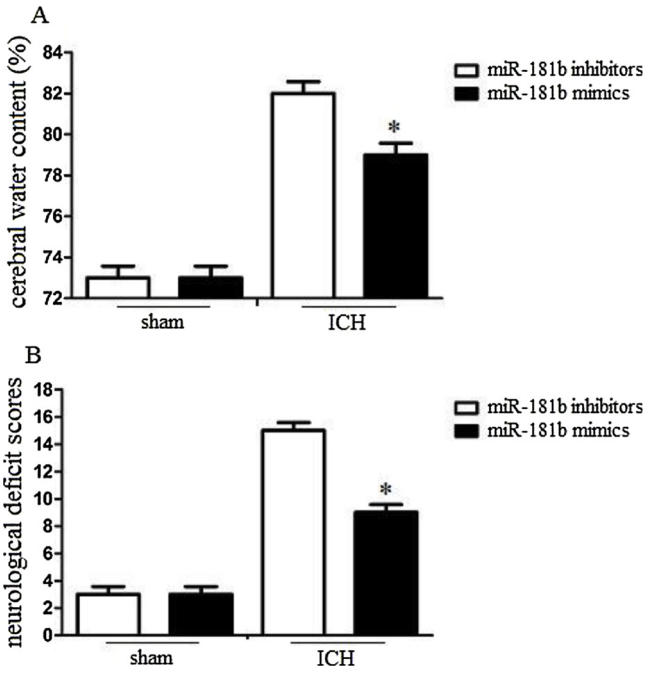

Fig. 7. miR-181b inhibited brain injury in ICH.
Mice were received an intracerebral ventricular injection of miR-181b mimics or inhibitors 10 min after ICH. (A) After 3 days following ICH, the cerebral water content of mice (n = 10 per group) was analyzed. (B) After 3 days following ICH, mice (n tests = 10 per group) were in a stable condition, and the neurological deficit were performed by behavioral measurement, including composite of motor, sensory, reflex, and balance tests. Experiments performed in triplicate showed consistent results. Data are presented as the mean ± SD of three independent experiments. *P < 0.05.

wet weight (wW) using an electronic analytic balance. After drying the brain hemisphere in an oven at 100 °C for 24 h, dry tissue weight (dW) was assessed. The percentage of water was calculated according to the following formula: brain water content (%) = (wW − dW)/wW × 100%.

2.20. Statistical analysis

Data are presented as mean ± SD. Statistical difference was determined by one-way ANOVA, followed by all pairwise multiple-comparison procedures with Bonferroni's test. Bar chart values were analyzed by Student's *t*-test. P < 0.05 was considered statistically significant.

3. Results

3.1. Erythrocyte lysates induced ER stress and damage of neurons in vitro

To identify whether erythrocyte lysates induced ER stress and damage of neurons in vitro, we analyzed the ultrastructure and cell viability of erythrocyte lysates treated neurons using electron microscopy and MTT assays. The data demonstrated that there was more lipid droplet formation in erythrocyte lysates group compared with PBS group (Fig. 1A). We also analyzed ER stress related protein CHOP and ATF4 levels. The data demonstrated that erythrocyte lysates promoted CHOP and ATF4 levels of neurons compared with PBS group (Fig. 1B). In addition, MTT assay demonstrated that erythrocyte lysates decreased neuron viability compared with PBS group (Fig. 1C). These findings indicated that erythrocyte lysates induced ER stress and damage of neurons in vitro.

3.2. Erythrocyte lysates downregulated miR-181b and upregulated HSPA5 levels of neurons

We detected miR-181b levels of neurons 48 h after erythrocyte lysates or PBS treatment. We found that miR-181b levels significantly decreased after erythrocyte lysates treatment. However, HSPA5 mRNA and protein levels increased after erythrocyte lysates treatment (Fig. 2). These results demonstrated that miR-181b and HSPA5 levels of neurons have an inverse correlation after erythrocyte lysates treatment.

3.3. HSPA5 was a direct target of miR-181b of neurons

The 3′-UTR of HSPA5 mRNA contains a putative miR-181b target sequence according to the target prediction program TargetScan (www.targetscan.org) (Fig. 3A). To prove HSPA5 was a direct target of miR-181b of neurons, we detected this relationship by a Dual-Luciferase reporter system. We found that co-expression with miR-181b mimics significantly suppressed the activity of a firefly luciferase reporter containing wild-type HSPA5 3′-UTR, while the phenomenon did not been detected on a reporter with a mutated HSPA5 3′-UTR (Fig. 3B). These results indicated that miR-181b likely attenuated HSPA5 expression by directly binding target sites in the HSPA5 3′-UTR. In addition, neurons were transduced with miR-181b mimics or inhibitors, and HSPA5 levels were analyzed with qRT-PCR and western blot assays. We found that transduction of miR-181b mimics enhanced miR-181b mRNA levels, while transduction of miR-181b inhibitors attenuated miR-181b mRNA expression. Moreover, miR-181b mimics significantly decreased HSPA5 levels (Fig. 3C).

3.4. miR-181b attenuated ER stress and damage of neurons in vitro

To further explore the role of miR-181b on ER stress and damage of neurons, we analyzed the ultrastructure and cell viability of erythrocyte lysates treated neurons using electron microscopy and MTT assays. miR-181b mimics or inhibitors transduction was performed to upregulate or knockdown miR-181b of neurons. We found that miR-181b mimics significantly attenuated lipid droplet formation and ER stress related protein CHOP and ATF4 levels (Fig. 4A-B). In addition, miR-181b mimics promoted neuron viability (Fig. 4C). The data demonstrated that miR-181b attenuated ER stress and damage of neurons in vitro.

3.5. miR-181b attenuated apoptosis of neurons in vitro

To analyze the role of miR-181b on apoptosis of neurons, we analyzed the cell apoptosis rate and specific apoptotic pathways. The results demonstrated miR-181b mimics significantly attenuated cell apoptosis rate and caspase-3 activity. However, miR-181b inhibitors increased cell apoptosis rate and caspase-3 activity (Fig. 5). Thus, the results demonstrated that miR-181b attenuated apoptosis of neurons in vitro.

3.6. miR-181b attenuated inflammation in vivo

Microglia infiltration is regarded as a hallmark to the brain inflammatory response. To detect the role of miR-181b in the microglia infiltration, we detected the Iba-1-positive microglia in the perihematomal brain tissues at 3 days after ICH. The results demonstrated that the number of microglia in the perihematomal brain tissues increased at 3 days after ICH compared with that in the sham group. However, administration of miR-181b significantly decreased the number of microglia in the perihematomal brain tissues (Fig. 6A). In addition, we also analyzed HSPA5, NF-κB p65, and inflammatory cytokine levels of perihematoma tissue of ICH mice. We found that administration of miR-181b significantly enhanced the miR-181b levels in vivo, and significantly attenuated HSPA5, NF-κBp65, IL-6, IL-1β, and TNF-α levels

in perihematoma tissue (Fig. 6B). These data demonstrated that miR-181b could attenuate inflammation in vivo.

3.7. miR-181b inhibited brain injury in ICH

To explore the role of miR-181b in brain injury, we also analyzed water content and neurological injury of ICH mice. We found that water content in mice brains and neurological injury significantly increased compared to sham-operated animals. However, administration of miR-181b significantly reduced water content and neurological injury (Fig.7). These data demonstrated that miR-181b could inhibit brain injury and enhance brain function after ICH.

4. Discussion

In this experiment, we provided the following evidence: (1) Erythrocyte lysates induced ER stress and damage of neurons in vitro; (2) Erythrocyte lysates downregulated miR-181b and upregulated HSPA5 levels of neurons; (3) miR-181b attenuated ER stress and damage of neurons via HSPA5 in vitro. (4) miR-181b attenuated inflammation and brain injury in ICH.

ICH is a main cause of death and long-term disabilities worldwide. Despite of numerous research and preclinical identification of neuroprotective chemicals, the available therapy for ICH is very limited [30]. Therefore, the development of other therapeutical strategy is in great needed. Much evidence shows that second inflammatory injury exerts an important role in neurological deficits following ICH [31–33]. However, the initiation induces innate immune and inflammatory responses have not been fully identified.

Related evidence demonstrates that the normal functioning of the ER in protein synthesis is disrupted and the ER switches to a stress state when cell experiences stress conditions [34]. The final consequence of ER stress determines cell death or cell survive [35]. It has been widely reported that ER stress is involved in ICH [36]. HSPA5, also called glucose-regulated protein of 78 kDa (GRP78), is a vital ER molecular chaperone and is regarded as a marker for ER stress [37]. Previous studies demonstrated that HSPA5 played a protective role in ischemia stroke [38]. Related evidence also suggested that upregulation of HSPA5 might contribute to parecoxib-mediated neuroprotection during ER stress responses [39]. Increased HSPA5 levels were also involved in astrocytes and neurons following ischemic treatment [40].

MicroRNAs (miRNAs) are characterized as small non-coding RNA molecules that negatively regulate protein expression in viruses, plants, and animals [41]. miRNAs can regulate the expression of genome and play an important effect in various biological processes, including cell differentiation, death, and metabolism [42]. However, the specific miRNAs regulates HSPA5 following ICH has not been well identified.

In this study, we identified an inverse relationship between miR-181b and HSPA5 expression. The 3′-UTR of HSPA5 mRNA contained conserved miR-181b binding sites, and we showed that miR-181b directly regulated HSPA5 expression through these 3′-UTR sites. Our results indicate that miR-181b downregulation leads to increased HSPA5 levels, ER stress and neuron damage following erythrocyte lysates treatment.

In addition, we also analyzed HSPA5, NF-κB p65, and inflammatory cytokine levels of perihematoma tissue of ICH mice. We found that administration of miR-181b significantly enhanced the miR-181b levels in vivo, and significantly attenauted HSPA5, NF-κBp65, IL-6, IL-1β, and TNF-α levels in perihematoma tissue. These data demonstrated that miR-181b could attenuate inflammation in vivo.

Lastly, we found that water content in mice brains and neurological injury significantly increased compared to sham-operated animals. However, administration of miR-181b significantly reduced water content and neurological injury. These data demonstrated that miR-181b could inhibit brain injury and enhance brain function after ICH.

In conclusion, our study demonstrated that miR-181b could attenuate brain injury through down-regulating HSPA5 protein levels in vitro and in vivo. In addition, decreased ER stress response might be one of the mechanisms underlying HSPA5 mediated neuron damage following ICH.

Acknowledgement

The study was supported by National Natural Science Foundation of China (NSFC No. 81870962).

References

[1] A.L. de Oliveira Manoel, A. Goffi, F.G. Zampieri, D. Turkel-Parrella, A. Duggal, et al., The critical care management of spontaneous intracranial hemorrhage: a contemporary review, Crit Care 20 (2016) 272.
[2] S.B. Murthy, A. Shastri, A.E. Merkler, D.F. Hanley, W.C. Ziai, et al., Intracerebral hemorrhage outcomes in patients with systemic cancer, J. Stroke Cerebrovasc. Dis. 25 (2016) 2918–2924.
[3] M.A. Topcuoglu, A.B. Singhal, Hemorrhagic reversible cerebral vasoconstriction syndrome: features and mechanisms, Stroke 47 (2016) 1742–1747.
[4] S.J. An, T.J. Kim, B.W. Yoon, Epidemiology, risk factors, and clinical features of intracerebral hemorrhage: an update, J. Stroke 19 (2017) 3–10.
[5] W. Ji, J. Wang, J. Xu, X. Zhao, X. Xu, et al., Lack of aquaporin 9 reduces brain angiogenesis and exaggerates neuronal loss in the hippocampus following intracranial hemorrhage in mice, J. Mol. Neurosci. 61 (2017) 351–358.
[6] Z. Fan, Y. Yuan, F. Wang, Y. Qi, H. Han, et al., Diabetes mitigates the recovery following intracranial hemorrhage in rats, Behav. Brain Res. 320 (2017) 412–419.
[7] G. Xi, J. Strahle, Y. Hua, R.F. Keep, Progress in translational research on intracerebral hemorrhage: is there an end in sight? Prog. Neurobiol. 115 (2014) 45–63.
[8] P. Yang, A. Manaenko, F. Xu, L. Miao, G. Wang, et al., Role of PDGF-D and PDGFR-beta in neuroinflammation in experimental ICH mice model, Exp. Neurol. 283 (2016) 157–164.
[9] Y. Zhang, Y. Chen, J. Wu, A. Manaenko, P. Yang, et al., Activation of dopamine D2 receptor suppresses neuroinflammation through alphaB-crystalline by inhibition of NF-kappaB nuclear translocation in experimental ICH mice model, Stroke 46 (2015) 2637–2646.
[10] M.L. Schmitz, M.S. Shaban, B.V. Albert, A. Gokcen, M. Kracht, The crosstalk of endoplasmic reticulum (ER) stress pathways with NF-kappaB: complex mechanisms relevant for cancer, inflammation and infection, Biomedicines 6 (2018).
[11] R. Higgins, J.M. Gendron, L. Rising, R. Mak, K. Webb, et al., The unfolded protein response triggers site-specific regulatory ubiquitylation of 40S ribosomal proteins, Mol. Cell 59 (2015) 35–49.
[12] K. Mishiba, Y. Nagashima, E. Suzuki, N. Hayashi, Y. Ogata, et al., Defects in IRE1 enhance cell death and fail to degrade mRNAs encoding secretory pathway proteins in the Arabidopsis unfolded protein response, Proc. Natl. Acad. Sci. U. S. A. 110 (2013) 5713–5718.
[13] K.M. Doyle, D. Kennedy, A.M. Gorman, S. Gupta, S.J. Healy, et al., Unfolded proteins and endoplasmic reticulum stress in neurodegenerative disorders, J. Cell. Mol. Med. 15 (2011) 2025–2039.
[14] X.M. Li, J. Liu, F.F. Pan, D.D. Shi, Z.G. Wen, et al., Quercetin and aconitine synergistically induces the human cervical carcinoma HeLa cell apoptosis via endoplasmic reticulum (ER) stress pathway, PLoS One 13 (2018) e0191062.
[15] Y. Cui, L. Ren, B. Li, J. Fang, Y. Zhai, et al., Melatonin relieves busulfan-induced spermatogonial stem cell apoptosis of mouse testis by inhibiting endoplasmic reticulum stress, Cell. Physiol. Biochem. 44 (2017) 2407–2421.
[16] W.W. Ma, L. Zhao, L.H. Yuan, H.L. Yu, H. Wang, et al., Elaidic acid induces cell apoptosis through induction of ROS accumulation and endoplasmic reticulum stress in SHSY5Y cells, Mol. Med. Rep. 16 (2017) 9337–9346.
[17] M. Niu, X. Dai, W. Zou, X. Yu, W. Teng, et al., Autophagy, endoplasmic reticulum stress and the unfolded protein response in intracerebral hemorrhage, Transl. Neurosci. 8 (2017) 37–48.
[18] X.C. Duan, W. Wang, D.X. Feng, J. Yin, G. Zuo, et al., Roles of autophagy and endoplasmic reticulum stress in intracerebral hemorrhage-induced secondary brain injury in rats, CNS Neurosci. Ther. 23 (2017) 554–566.
[19] C. Guo, Y. Geng, F. Song, Y. Huo, X. Wu, et al., Mild hypothermia protects rat neuronal injury after intracerebral hemorrhage via attenuating endoplasmic reticulum response induced neuron apoptosis, Neurosci. Lett. 635 (2016) 17–23.
[20] D.S. Li, J.L. Ainiwaer, I. Sheyhiding, Z. Zhang, L.W. Zhang, Identification of key long non-coding RNAs as competing endogenous RNAs for miRNA-mRNA in lung adenocarcinoma, Eur. Rev. Med. Pharmacol. Sci. 20 (2016) 2285–2295.
[21] M. Matsui, T.P. Prakash, D.R. Corey, Argonaute 2-dependent regulation of gene expression by single-stranded miRNA mimics, Mol. Ther. 24 (2016) 946–955.
[22] J.Y. Tan, A.C. Marques, miRNA-mediated crosstalk between transcripts: the missing "linc"? Bioessays 38 (2016) 295–301.
[23] J. Niu, J. Wang, J. An, L. Liu, Z. Lin, et al., Integrated mRNA and miRNA transcriptome reveal a cross-talk between developing response and hormone signaling for the seed kernels of Siberian apricot, Sci. Rep. 6 (2016) 35675.
[24] L. Qun, X. Wenda, S. Weihong, M. Jianyang, C. Wei, et al., miRNA-27b modulates endothelial cell angiogenesis by directly targeting Naa15 in atherogenesis, Atherosclerosis 254 (2016) 184–192.
[25] S.D. Alipoor, E. Mortaz, J. Garssen, M. Movassaghi, M. Mirsaeidi, et al., Exosomes

and exosomal miRNA in respiratory diseases, Mediators Inflamm. 2016 (2016) 5628404.
[26] Y. Zhang, B. Han, Y. He, D. Li, X. Ma, et al., MicroRNA-132 attenuates neurobehavioral and neuropathological changes associated with intracerebral hemorrhage in mice, Neurochem. Int. 107 (2017) 182–190.
[27] J.M. Kim, S.T. Lee, K. Chu, K.H. Jung, J.H. Kim, et al., Inhibition of Let7c microRNA is neuroprotective in a rat intracerebral hemorrhage model, PLoS One 9 (2014) e97946.
[28] Y. Bai, L. Wang, L. Sun, P. Ye, R. Hui, Circulating microRNA-26a: potential predictors and therapeutic targets for non-hypertensive intracerebral hemorrhage, Med. Hypotheses 77 (2011) 488–490.
[29] Z. Yang, L. Zhong, R. Xian, B. Yuan, MicroRNA-223 regulates inflammation and brain injury via feedback to NLRP3 inflammasome after intracerebral hemorrhage, Mol. Immunol. 65 (2015) 267–276.
[30] K.E. Wartenberg, S.A. Mayer, Reducing the risk of ICH enlargement, J. Neurol. Sci. 261 (2007) 99–107.
[31] H. Wu, T. Wu, W. Hua, X. Dong, Y. Gao, et al., PGE2 receptor agonist misoprostol protects brain against intracerebral hemorrhage in mice, Neurobiol. Aging 36 (2015) 1439–1450.
[32] Y. Zhou, Y. Wang, J. Wang, R. Anne Stetler, Q.W. Yang, Inflammation in intracerebral hemorrhage: from mechanisms to clinical translation, Prog. Neurobiol. 115 (2014) 25–44.
[33] H. Fang, P.F. Wang, Y. Zhou, Y.C. Wang, Q.W. Yang, Toll-like receptor 4 signaling in intracerebral hemorrhage-induced inflammation and injury, J. Neuroinflammation 10 (2013) 27.
[34] Y. Taguchi, Y. Horiuchi, F. Kano, M. Murata, Novel prosurvival function of Yip1A in human cervical cancer cells: constitutive activation of the IRE1 and PERK pathways of the unfolded protein response, Cell Death Dis. 8 (2017) e2718.
[35] S.J. Tavernier, F. Osorio, L. Vandersarren, J. Vetters, N. Vanlangenakker, et al., Regulated IRE1-dependent mRNA decay sets the threshold for dendritic cell survival, Nat. Cell Biol. 19 (2017) 698–710.
[36] C. Meng, J. Zhang, B. Dang, H. Li, H. Shen, et al., PERK pathway activation promotes intracerebral hemorrhage induced secondary brain injury by inducing neuronal apoptosis both in vivo and in vitro, Front. Neurosci. 12 (2018) 111.
[37] M. Cerezo, S. Rocchi, New anti-cancer molecules targeting HSPA5/BIP to induce endoplasmic reticulum stress, autophagy and apoptosis, Autophagy 13 (2017) 216–217.
[38] P. Wang, N. Zhang, J. Liang, J. Li, S. Han, Micro-RNA-30a regulates ischemia-induced cell death by targeting heat shock protein HSPA5 in primary cultured cortical neurons and mouse brain after stroke, J. Neurosci. Res. 93 (2015) 1756–1768.
[39] Z. Ye, N. Wang, P. Xia, E. Wang, J. Liao, et al., Parecoxib suppresses CHOP and Foxo1 nuclear translocation, but increases GRP78 levels in a rat model of focal ischemia, Neurochem. Res. 38 (2013) 686–693.
[40] A. Benavides, D. Pastor, P. Santos, P. Tranque, S. Calvo, CHOP plays a pivotal role in the astrocyte death induced by oxygen and glucose deprivation, Glia 52 (2005) 261–275.
[41] M. Martinez-Pacheco, A. Hidalgo-Miranda, S. Romero-Cordoba, M. Valverde, E. Rojas, MRNA and miRNA expression patterns associated to pathways linked to metal mixture health effects, Gene 533 (2014) 508–514.
[42] M. D'Anzeo, L. Faloppi, M. Scartozzi, R. Giampieri, M. Bianconi, et al., The role of micro-RNAs in hepatocellular carcinoma: from molecular biology to treatment, Molecules 19 (2014) 6393–6406.